FINESSE: The Next Generation

Ian Charles Waters, III

Central Connecticut State University

July 31, 2018

Abstract

In stark contrast to the incredibly energetic astrophysical events associated with their creation, the gravitational waves emitted by these events are almost unimaginably small and thus notoriously difficult to detect. The effort to study them has resulted in the creation of ever larger and more complex interferometers. FINESSE is precision software used by the gravitational wave community in modelling these and other optical systems. Originally developed over twenty years earlier, FINESSE is currently undergoing a rewrite in order to meet some of the challenges faced with modeling the next generation of gravitational wave detectors. One of the planned features, not found in earlier versions, is the ability to model polarization. This paper will examine in some detail some of the underlying mathematics, history, and detection of gravitational waves, including both Michelsen and Sagnac interferometers. It will then explore the polarization of light and how it was implemented into the upcoming version of FINESSE and how this will help researchers prepare for the future of gravitational wave detection.

I. Introduction

It was in 1974, that graduate student Russell Alan Hulse and his thesis advisor Joseph Hooton Taylor, Jr., both then of the University of Massachusetts, Amherst, were in Puerto Rico working on a large-scale sky survey using the Arecibo Observatory's 305 meter radio telescope. The pair were quite busy searching for pulsars, rapidly rotating and highly magnetized neutron stars that emit electromagnetic pulses at regular intervals, typically in the form of radio waves in the direction of detectors here on earth. It was upon carefully analyzing some of their data that Hulse and Taylor noticed something quite pecuiliar. One source in particular had a most usual variation in the timing of its pulses, and upon carfeful consideration the pair ddetermined that this unexpected result might best be explained by a neutron star in a binary orbit with some other object around a common center of mass, later confirmed to be a secondary neutron star. This marked the discovery of the first binary pulsar[1].

Additional observations of the system, which subsequently came to be known as the Hulse-Taylor binary, revealed something even more extraordinary. The orbits of the stars were found to be contracting over time, and it was generally thought that this was due to the radiation of energy away from the system in the form of gravitational waves, a series of disturbances in the fabric of spacetime which propagate outward from their source at the speed of light. This discovery then marked the first indirect evidence of the existence of gravitational waves, as originally predicted by Albert Einstein many years earlier as a consequence of his General Theory of Relativity[2].

A number of years later, on February 11th, 2016, the LIGO collaboration announced to the world the first direct detection of gravitational waves using LIGO's massive gravitational wave interferometers[3].

LIGO, otherwise known as the Laser Interferometer Gravitational-Wave Observatory, is currently the most sensitive gravitational wave-detector in the world, consisting of one detector in Livingston, Louisiana, and two in Richland, Washington. Having interferometers in different locations provides researchers a rough estimate as to the origin of the oncoming wave.

The event, GW150914, was the result of two merging black holes of 29 and 36 solar masses,

into a single 62 solar mass black hole. As a result, approximately 3 solar masses was converted into energy and radiated away in the form of gravitational waves. These waves then travelled some 1.3 billion light years across the vastness of space before changing the test masses in LIGO's detectors by about one 200th the charge diameter of a proton[3]. Several months later on June 15, 2016, LIGO announced the detection of a secondary event, GW151226, which was also the result of a black hole merger [4].

Indeed, the events leading up to the first direct detection by LIGO in 2015 is marked by a multinational effort involving decades of work using increasingly larger and more complex interferometers. This has, in turn, created a need to be able to model both these systems and other optical configurations using software[5].

To meet this demand, in 1997 Professors Andreas Freise and Gerhard Heinzel began developing FINESSE, advanced numerical software for modelling interferometric systems. FINESSE has been continuously developed since then, and the third version is currently being readied for release. FINESSE 3 will contain a number of features not found in earlier versions, including the ability to implement polarization.

In this paper we begin by looking at some of the basic mathematics of gravitational waves, as predicted by the linearized Einstein equation. We then move onto a different type of wave, electromagnetic waves, where we find that combining them in specific waves produces various forms of polarized light. We then briefly examine polarizers and the role of the Jones calculus in calculating various states of polarization. Finally, we examine in some detail how polarization was actually implemented in Finesse.

II. Narrative

i. Linearized Gravitational Waves

At the center of the general theory of relativity are *Einstein's field equations*, a set of ten partial differential equations that together describe gravitation as a curvature of spacetime in the presence of mass and energy:

$$R_{\mu\nu} - \frac{1}{2}g_{\mu\nu}R = \frac{8\pi G}{c^4}T_{\mu\nu} \tag{1}$$

where G and c are the gravitational constant and speed of light in a vacuum, respectively. The quantities $R_{\mu\nu}$, R, $g_{\mu\nu}$, and $T_{\mu\nu}$, known as the *Ricci tensor*, *scalar curvature*, *metric tensor*, and *stress energy tensor* respectively, represent several different geometric objects known as *tensors*. Tensors are functions which describe linear relations between scalars, vectors, and other tensors (the vector dot and cross products are two readily familiar examples). More generally, a tensor is a function which maps vectors and one-forms to the real numbers.

Typically, one is interested in solving the field equations for the metric tensor $g_{\mu\nu}$, which itself describes how geometric quantities such as lengths and angles are determined within a spacetime corresponding to some particular arrangement of mass and energy. In tensor calculus, it is customary to forego the usual sigma summation notation in favor of the appreciably more compact Einstein summation convention, where any index variable appearing twice in a given term is summed over all values of its index. Using this convention, we can then express a line element g formed of $i \times j$ terms as

$$g = g_{ij}dx^i dx^j \tag{2}$$

For the sake of illustration, consider the infinitesimal spacetime interval ds described in Einstein's special theory of relativity, also known as the *Minkowski metric*:

$$ds^2 = -c^2dt + dx^2 + dy^2 + dz^2 \tag{3}$$

Using the Einstein summation convention, we can more compactly express (3) as

$$ds^2 = \eta_{\mu\nu}dx^\mu dx^\nu \tag{4}$$

Note here that $\eta_{\mu\nu}$ is a 4×4 matrix corresponding to the four dimensions of spacetime:

$$\eta_{\mu\nu} = \begin{bmatrix} -c^2 & 0 & 0 & 0 \\ 0 & 1 & 0 & 0 \\ 0 & 0 & 1 & 0 \\ 0 & 0 & 0 & 1 \end{bmatrix} \tag{5}$$

The Minkowski metric is part of a family of known solutions to the field equations known as the *vacuum solutions*, and can be found by solving for a spacetime in the absence of mass or energy.

Another vacuum solution of interest is the *Schwarzchild metric*, which describes the curvature of spacetime in the presence of massive, non-rotating astrophysical bodies such as stars or black holes. This metric is found by solving the field equations for a spherically symmetric distribution of mass. On the other hand, solutions to the field equations for masses in non-uniform motion, including the aforementioned Hulse-Taylor binary, describe freely propagating gravitational waves.

Owing to the incredible distances through which these disturbances propagate between their far-away astrophysical sources and detectors on earth, the amplitude of these waves is considerably small. As such, we can begin with a known solution to the field equations, the Minkowski metric, and make a suitable linear approximation to arrive at a new metric describing the spacetime geometry associated with our waves, saving us a considerable amount of mathematical legwork. We use an approach similar to James B. HartleâĂŹs in his text *Gravity: An Introduction to General Relativity*. [6].

We consider now an otherwise flat spacetime through which a series of very small perturbations $h_{\mu\nu}(t,z)$ propagate in the positive z direction as the result of some far off cosmic event, where

$$h_{\mu\nu}(t,z) = \begin{bmatrix} 0 & 0 & 0 & 0 \\ 0 & 1 & 0 & 0 \\ 0 & 0 & -1 & 0 \\ 0 & 0 & 0 & 0 \end{bmatrix} f(t-z) \tag{6}$$

with the restriction that $|f(t-z)| \ll 1$.

Given that the spacetime we are considering is at least *close* to being flat, we can write a metric $g_{\mu\nu}$ describing this geometry as

$$g_{\mu\nu} = \eta_{\mu\nu} + h_{\mu\nu}(t,z) \tag{7}$$

The behavior of spacetime in the presence of the perturbations may perhaps best be understood by considering the subsequent motion of a series of test masses relative to one another. We imagine now two light test particles, one at the origin and second situated on the x-axis some distance L_0 away (as measured in unperturbed, flat spacetime). The motion of the particles can then be found by solving the *geodesic equation* using $g_{\mu\nu}$, which describes the trajectories of free particles in spacetime:

$$\frac{\partial^2 x^i}{\partial \tau^2} + \Gamma^i_{\alpha\beta} \frac{\partial x^\alpha}{\partial \tau} \frac{\partial x^\beta}{\partial \tau} = 0 \tag{8}$$

where τ is the proper time of the particle, and

$$\Gamma^i_{\alpha\beta} = \frac{\partial \mathbf{e}_\alpha}{\partial x^\beta} \cdot g^{i\gamma} \mathbf{e}_\gamma \tag{9}$$

It can be shown that the Christoffel symbol of the second kind $\Gamma^i_{\alpha\beta}$ vanishes in Minkowski space. Owing to this result, we then find that for some first order change δx^i in x^i:

$$\frac{\partial^2 \delta x^i}{\partial \tau^2} = 0 \tag{10}$$

When we consider this result along with the fact that the particles are initially at rest, we find that for all times τ that

$$\delta x^i(\tau) = 0 \tag{11}$$

where we see that the coordination postions of the test masses remain unaffected throughout the passage of the wave. The same is not true for their separation distance, however, as we will now see.

Recall the earlier separtion distance L_0 of the two particles in the unperturbed flat spacetime. In the spacetime of the wave, however, the separation distance $L(t)$ of the two particles can be found by evaluating

$$L(t) = \int_0^L dx\sqrt{1 + h_{xx}(t,0)} \approx L + \frac{L}{2}h_{xx}(0,t) \tag{12}$$

We then solve for the fractional change in length $\frac{\delta L(t)}{L_0}$, also known as the *shear*:

$$\frac{\delta L(t)}{L_0} = \frac{1}{2}h_{xx}(t,0) \tag{13}$$

This demonstrates that the separation distance of the two test particles changes over time as the wave passes, even as their coordinate positions remain unaffected. If the wave has some amplitude A, frequency ω, and phase shift ϕ such that $f(t-z) = A\sin[\omega(t-z)+\phi]$, then the shear becomes

$$\frac{\delta L(t)}{L_0} = \frac{1}{2}A\sin(\omega t + \phi) \tag{14}$$

which demonstrates that the shear in the x-direction oscillates with half of the original amplitude of the wave. This relation also provides a hint as to how we might detect gravitational waves in practice, an idea that we will visit in detail in the next section.

We consider now a situation in which we employ a large number of particles arranged in a circle in the xy-plane with the origin at the center. To determine how distances between each particle and the origin might change as a wave of the form $f(t-z) = A\sin[\omega(t-z)+\phi]$ passes along in the positive z-direction, we introduce new coordinates X and Y as follows:

$$\begin{aligned} X(t,x) &= \Big(1 + \frac{1}{2}A\sin(\omega t)\Big)x \\ Y(t,y) &= \Big(1 - \frac{1}{2}A\sin(\omega t)\Big)y \end{aligned} \tag{15}$$

Observe that although X and Y vary as a function of time t, that the original unperturbed x and y coordinates of the test particles do not. One is then able to determine the separation distances in this new coordinate system using basic plane geometry.

We now note that although the perturbed metric $g_{\mu\nu}$ is an approximate solution to the field equations, it is not the most general solution possible. In fact, $g_{\mu\nu}$ represents just one of two possible independent polarizations of a gravitational wave, the first of which is typically call the $+$ (plus) polarization. In order to find the second, we begin by rotating the xy-plane clockwise by some arbitary angle (for the sake of illustration we choose π 4 radians), and then proceed to determine a relation between the original coordinates, x and y, and the rotated coordinates, x' and y' :

$$\begin{aligned} x &= \frac{\sqrt{2}}{2}(x' + y') \\ y &= \frac{\sqrt{2}}{2}(x' - y') \end{aligned} \tag{16}$$

We now substitute these relations into the perturbed metric $g_{\mu\nu}$, where we find that the flat spacetime component $\eta_{\mu\nu}$ is unaffected by the rotation. For the $h_{\mu\nu}$ representing the wave, we observe that:

$$\begin{aligned} h_{x'x'} &= 0 \\ h_{x'y'} = h_{y'x'} &= h_{xx} = -h_{yy} \\ h_{y'y'} &= 0 \end{aligned} \tag{17}$$

We have now a second polarization, linearly independent of the first, typically called the $\times$ (cross) polarization:

$$h_{\mu\nu}(t,z) = \begin{bmatrix} 0 & 0 & 0 & 0 \\ 0 & 0 & 1 & 0 \\ 0 & 1 & 0 & 0 \\ 0 & 0 & 0 & 0 \end{bmatrix} f(t-z) \tag{18}$$

Owing to this linear independence, we find that the most general linearized gravitational wave is a superposition of metric perturbations:

$$h_{\mu\nu}(t,z) = \begin{bmatrix} 0 & 0 & 0 & 0 \\ 0 & f_+(t-z) & f_\times(t-z) & 0 \\ 0 & f_\times(t-z) & -f_+(t-z) & 0 \\ 0 & 0 & 0 & 0 \end{bmatrix} \tag{19}$$

for some functions $f_+(t-z)$ and $f_\times(t-z)$.

ii. The Michelson Interferometer

In order to understand how gravitational waves might be detected using interferometers, we once again begin by considering a series of test masses.

Imagine now that the first particle is located at the origin in the horizontal xy-plane, where it supports both a beam splitter and detector. A further two particles we place some distance away, with the first secured at some distance L_x away along the positive x-axis, and the second positioned at some distance L_y along the positive y-axis, such that the three particles along with the portions of the x and y-axes connecting them form a basic "L" shape . Finally, imagine that the particles on the x and y axes each support a mirror directly facing the first particle situated at the origin.

Now we imagine that a laser is introduced into the beam splitter of the first particle from some outside source. The incident beam is divided and redirected, with one beam heading along in the positive x-direction, and the second along in the positive y-direction. The two beams strike the mirrors supported by the other masses, and are reflected back along the same axes towards the detector at the origin, where they are recombined to produce an interference pattern that can then be analyzed. This is the design of a basic Michelson interferometer.

We observe that the resulting interference pattern will be constructive if the lengths of the two arms L_x and L_y differ by some integer multiple n of the wavelength of the laser λ. Similarly, this interference will be destructive if L_x and L_y differ by some odd number of half-wavelengths.

We consider once again how our imagined system would be affected if a gravitational wave of some amplitude A, frequency ω, and phase shift ϕ such that $f(t-z) = A\sin[\omega(t-z)+\phi]$ passes through the region containing the interferometer in the positive z-direction. As the wave passes, the distances L_x and L_y will alternately expand and contract as

$$\begin{aligned} \frac{\delta L_x(t)}{L_x} &= \frac{1}{2}A\sin(\omega t+\phi) \\ \frac{\delta L_y(t)}{L_x} &= -\frac{1}{2}A\sin(\omega t+\phi) \end{aligned} \tag{20}$$

which will in turn affect the resulting interference pattern, which will begin to cycle through the conditions for constructive and destructive interference. The resulting amplitude A and frequency ω of the passing wave can then be determined through the careful examination of this resulting interference pattern.

It then follows from (20) that at least generally speaking, the larger the dimensions of the interferometer, the greater the change in resulting interference pattern for a given wave, and ultimately the more effective the apparatus can be at gravitational wave detection. This is precisely the reason that gravitational wave detectors like LIGO are so large. Two of LIGOâĂŹs three detectors feature orthogonal arms 4 km in length, arranged in the same basic configuration as our own imagined interferometer. Using these dimensions, LIGO is then able to detect a change in beam spacing less than one ten-thousandth the charge diameter of a proton, equivalent to accurately determining the distance from Earth to the nearest star Proxima Centauri, some 4×10^{13} kilometers away, by less than the width of a human hair.

Although considerably more sophisticated, modern day *dual-recycled Michelson interferometers* like LIGO work in much of the same way as the original Michelson design, employing additional cavities in each of their two orthogonal arms. These cavities each consist of an additional test mass supporting a mirror with a relatively low coefficient of reflection. Tuned to resonance, the cavities then behave as if there

were multiple reflections of the beam from one end of each arm to the origin before recombination, increasing the effective length of the interferometer, and ultimately, its sensitivity to gravitational wave signals.

Despite its trememdous successes in recent years, however, like all tools used in experimental endeavors LIGO is not without inherent limitations. In particular, the sensitivity required to test Einstein's theory of gravity in strong field conditions, or to realize a precision gravitational wave astronomy, exceed the expected performance of both its advanced detectors and planned upgrades. For instance, LIGO is particularly susceptible to seismic, gravitational gradient, and thermal noises of the suspension and test masses and as such its performance is limited at lower frequencies.

In order to address a number of these concerns, a third-generation gravitational wave detector known as the Einstein Telescope is currently being considered for development by several institutions in the European Union, among them the University of Birmingham, University of Glasgow, and Cardiff University. The Einstein Telescope is expected to be built underground in an effort to minimize seismic and gravitational gradient noise. It will also be considerably larger than LIGO, featuring three arms 10 kilometers in length arranged in an equilateral triangle, along with two detectors in each of the three corners.

Owing to its ambitious design, The Einstein Telescope is expected to be ten times as sensitive to prospective signals as Advanced LIGO, in addition to being able to measure of incoming gravitational wave polarization. The current design includes three nested detectors, each composed of two Michelson interferometers, each optimized for either low or high frequencies.

iii. The Sagnac Interferometer

The natural ability of the Michelson to provide differential length measurements indeed suggest it the sensible choice to incorporate into the Einstein Telescope's design as a replacement for the low-frequency portion of its detectors, which seems to offer a number of advantages not to be found in the Michelson design. This includes a similar level of radiation pressure noise suppression without any need for a signal recycling mirror or extensive filtering cavities[8].

The *Sagnac effect*, named for French physicist Georges Sagnac, is an optical phenomenon encountered in interferometry as a result of rotation. This effect can readily be seen in a ring interferometer consisting of a laser that is directed into a beamsplitter and the two beams redirected to follow the same optical path, albeit in opposite directions. Upon returning to the beamsplitter, the two beams exit the beamsplitter where they recombine and produce interference patterns. Both the phase angle of the beams and resulting interference patterns are affected by the angular velocity of the system, in accordance with Einstein's special theory of relatvity.

It can be shown that for an arbitarily-shaped Sagnac interferometer enclosing an area A and with angular velocity $\vec{\omega}$, the fringe displacement $\Delta\phi$ is

$$\Delta\phi = \frac{4\pi A}{\lambda c}\vec{\omega} \cdot \mathbf{e}_n \tag{21}$$

where λ is the original wavelength of the laser, c is the speed of light in a vacuum, and $\mathbf{e}_n$ is a unit vector normal to the Gaussian surface formed by the path of the laser.

As a common path interferometer, the inherent geometry of the Sagnac design matches the path lengths of the two beams, and as a result are almost completely insensitive to displacements of optical components. This desirable characteristic has led to the use of the design in applications requiring a high degree of stability.

As can be seen in (21) above, the resultant fringe displacement $\Delta\phi$ is directly proportional to the enclosed area of the path of the beam, and is specified in relation to the axis of rotation of the interferometer. The sign is then changed if the optical path is reversed in the opposite direction. Thus an optical path that

features loops in both directions has a net area given by the difference in the areas of the two loops. In the case that the area of the two loops is equal, the result is known as a *zero-area Sagnac interferometer*, a configuration that maintains the stability of the original Sagnac design, although is unaffected by rotation.

In order to minimize changes to the proposed design of the Einstein Telescope, the implementation of a Sagnac interferometer might best be achieved through the addition of polarizing beam splitters and quarter-wave plates. We now will be taking a closer look at both polarizing optical components and the polarization of light in general.

iv. The Polarization of Light

In order to determine how we might implement polarization into FINESSE, we must first understand some of the mathematics of polarized light. What follows is a treatment similar to Eugene Hecht's in his text *Optics*.[7]

Consider a plane electromagnetic wave which propagates through space in the positive z-direction of frequency ν, characterized by its electric field component $\vec{E}_x$ as

$$\vec{E}_x(z,t) = \boldsymbol{e}_x E_{x0} \exp[i(kz - \omega t)] \tag{22}$$

where $k = 2\pi\nu/c$, $\omega = 2\pi\nu$, and $\boldsymbol{e}_x$ is a unit vector parallel to the x-axis.

Note that the orientation of $\vec{E}$ is constant as a function of both time and postion, and as such we refer to the wave as being *linearly polarized*. Furthermore, we observe that $\vec{E}$ as well as the wave vector $\vec{k} = \boldsymbol{e_k}\omega/c$, oriented in the direction of the propagation of the wave reside in the same plane. This is typically referred to as the *plane of vibration*.

We imagine now a second wave in addition to the first, of the same frequency ν, which also propagates in the positive z-direction such that the two waves share the same wave vector $\vec{k} = \boldsymbol{e_k}\omega/c$, albeit with mutually orthogonal electric field component vectors:

$$\vec{E}_y(z,t) = \boldsymbol{e}_y E_{y0} \exp[i(kz - \omega t)] \tag{23}$$

Here $\boldsymbol{e}_y$ is a unit vector parallel to the y-axis. Similar to the first, this wave is linearly polarized as well.

We consider now the general case where the waves are out of phase with one another, which we account for by introducing a phase shift ϕ into the equation given for $\vec{E}_y$ in (23). We then express the two waves as

$$\vec{E}_x(z,t) = \boldsymbol{e}_x E_{x0} \exp[i(kz - \omega t)] \tag{24}$$

$$\vec{E}_y(z,t) = \boldsymbol{e}_y E_{y0} \exp[i(kz - \omega t + \phi)] \tag{25}$$

These two waves then combine to form a single wave $\vec{E}$, which is the simple vector summation of (24) and (25):

$$\vec{E}(z,t) = \vec{E}_x(z,t) + \vec{E}_y(z,t) \tag{26}$$

This resultant wave is linearly polarized as well, and is observed with its electric field vector $\vec{E}$ oscillating about a line rotated away from the x-axis by some angle $\theta = \arctan(E_{y0}/E_{x0})$ in the xy-plane. Furthermore, its amplitude E can be calculated as

$$E(z,t) = \sqrt{[E_x(z,t)]^2 + [E_y(z,t)]^2} \tag{27}$$

It is important to emphasize here that this process might also be carried about in reverse, where we able to resolve any plane-polarized wave into two orthogonal components. Indeed, by convention we refer to the linear polarization component in the plane of incidence as the *p-polarization*, and the component orthogonal to this plane as the *s-polarization*.

We observe now that in the case where ϕ is zero or some even integer multiple of π, that equation (26) becomes

$$\vec{E}(z,t) = (\boldsymbol{e_x} E_{x0} + \boldsymbol{e_y} E_{y0}) \exp[i(kz - \omega t)] \tag{28}$$

and $\vec{E}_x$ and $\vec{E}_y$ are in phase.

In the case where ϕ is some odd nonzero integer multiple of π, equation (26) becomes

$$\vec{E}(z,t) = (\boldsymbol{e_x}E_{x0} - \boldsymbol{e_y}E_{y0})\exp[i(kz-\omega t)] \tag{29}$$

Consider now a case where the waves $\vec{E}_x$ and $\vec{E}_y$ have equal magnitudes such that $E_{x0} = E_{y0} = E_0$, and phase shift $\phi = -\pi/2 \pm 2n\pi$, for some integer n. We can then express the real parts of equations (22) and (23) as

$$\vec{E}_x(z,t) = \boldsymbol{e}_x E_0 \cos(kz-\omega t) \tag{30}$$
$$\vec{E}_y(z,t) = \boldsymbol{e}_y E_0 \sin(kz-\omega t) \tag{31}$$

The resultant wave $\vec{E}$ is now

$$\vec{E}(z,t) = \boldsymbol{e}_x E_0 \cos(kz-\omega t) + \boldsymbol{e_y} E_0 \sin(kz-\omega t) \tag{32}$$

For some position on the z-axis, the magnitude of $\vec{E}$ remains fixed at E_0 for all times t, as the angle formed by $\vec{E}$ and the x-axis θ varies as $\theta = \omega t$. To an observer situated on the positive x-axis to whom the wave is propagating, $\vec{E}$ appears to be rotating clockwise, thus we say that the resultant wave is *right-circularly polarized*.

On the other hand, if the phase shift $\phi = \pi/2 \pm 2n\pi$ for some integer n, the real parts of equations (22) and (23) become

$$\vec{E}_x(z,t) = \boldsymbol{e_x} E_0 \cos(kz-\omega t) \tag{33}$$
$$\textit{and} \quad \vec{E}_y(z,t) = -\boldsymbol{e_y} E_0 \sin(kz-\omega t) \tag{34}$$

and the resultant wave $\vec{E}$ is now

$$\vec{E}(z,t) = \boldsymbol{e_x} E_0 \cos(kz-\omega t) - \boldsymbol{e_y} E_0 \sin(kz-\omega t) \tag{35}$$

To the same observer situated on the positive x-axis, $\vec{E}$ would now appear to be rotating clockwise, and we now say that the resultant wave is *left-circularly polarized*.

Interestingly, a linearly polarized wave can in some conditions be created through the addition of two circularly polarized waves. In particular, if we add the waves described in equations (32) and (35) above, we find that

$$\vec{E}(z,t) = \boldsymbol{e_x} 2E_0 \cos(kz-\omega t) \tag{36}$$

which is a linearly polarized wave of the same form as that of the real part of equation (1).

In the preceding pages we considered first the case where the electric field vector $\vec{E}$ was free to change its magnitude as a function of time t, as its angle with an arbitary axis remained constant (linear polarization). In contrast, we then considered the case where the magnitude of $\vec{E}$ remain fixed as its angle changed at some constant angular speed ω (circular polarization). It seems reasonable then to consider a third case where we allow both the magntidue and angle of $\vec{E}$ to vary over time, where the endpoint of $\vec{E}$ will trace out an ellipse in a plane perpendicular to the progation of the wave.

In order to show that the trace of $\vec{E}$ is indeed an ellipse, we begin by again considering the magnitudes of the real parts of equations (22) and (23):

$$E_x(z,t) = E_{x0}\cos(kz-\omega t) \tag{37}$$
$$E_y(z,t) = E_{y0}\cos(kz-\omega t+\phi) \tag{38}$$

We then use the sum formula for cosines to rewrite (38) as

$$E_y(z,t) = E_{y0}\cos(kz-\omega t)\ cos\phi - E_{y0}\sin(kz-\omega t)\ sin\phi \tag{39}$$

We then combine equations (37) and (39) to obtain

$$\frac{E_y}{E_{y0}} - \frac{E_x}{E_{x0}} cos\phi = -\sin(kz-\omega t) sin\phi \tag{40}$$

It then follows from (37), that

$$\sin(kz-\omega t) = \sqrt{1-\left(\frac{E_x}{E_{x0}}\right)^2} \tag{41}$$

and

$$\Big(\frac{E_y}{E_{y0}} - \frac{E_x}{E_{x0}} cos\phi\Big)^2 = \Big[1 - \Big(\frac{E_x}{E_{x0}}\Big)^2\Big] \sin^2\phi \tag{42}$$

Finally, upon solving (42) for $\sin^2\theta$ and rearranging, we find that:

$$\Big(\frac{E_y}{E_{y0}}\Big)^2 - \Big(\frac{E_x}{E_{x0}}\Big)^2 - 2\Big(\frac{E_y}{E_{y0}}\Big)\Big(\frac{E_x}{E_{x0}}\Big)\cos\phi = \sin^2\phi \tag{43}$$

which is the equation of an ellipse centered at the origin and rotated counterclockwise by some angle θ, where

$$\theta = \frac{1}{2} tan^{-1}\Big(\frac{2E_{x0}E_{y0}\cos\phi}{E_{x0}^2 - E_{y0}^2}\Big) \tag{44}$$

Observe that in the case where ϕ is zero or some even integer multiple of π, that (43) reduces to

$$E_y = \frac{E_{y0}}{E_{x0}} x \tag{45}$$

which is the equation of the same line described in equation (28).

In the case where ϕ is some odd non-zero integer multiple of π, (43) reduces to

$$E_y = -\frac{E_{y0}}{E_{x0}} x \tag{46}$$

which is the equation of the line described in equation (29).

In the case where $E_{x0} = E_{y0} = E_0$ and the phase shift $\phi = \pm\pi/2 + 2n\pi$, for some integer n, (43) reduces to

$$E_x^2 + E_y^2 = E_0^2 \tag{47}$$

which is the equation of the same circles described in equations (32) and (35).

This effectively demonstrates that both linearly and circularly polarized waves are specific cases of a much more general*elliptical polarization*. Describing a given wave as linearly, circularly, or elliptically polarized is known as its *state of polarization*.

As we have seen, information about a particular state of polarization is specified by both the amplitude and phase of oscillation in the electric field vector $\vec{E}$ components $\vec{E}_x$ and $\vec{E}_y$, given in a plane perpendicular to the propagation of the wave, as in equation (26). We may also express (26) equivalently as a two-dimensional *Jones Vector*:

$$\vec{E} = \begin{bmatrix} E_x \\ E_y \end{bmatrix} = \begin{bmatrix} E_{x0}\exp\left(i[kz - \omega t)\right] \\ E_{y0}\exp\left(i[kz - \omega t + \phi]\right) \end{bmatrix} \tag{48}$$

A *polarizer* is a type of optical filter which permits waves of a particular polarization to pass while restricting waves of other polarizations. Polarizers may generally be divided into two categories: *absorptive polarizers*, where undesired polarization states are absorbed by the device, and *beam-splitting polarizers*, which divide an unpolarized wave into two waves with opposite polarization states.

Consider a linearly polarized wave $\vec{E}_{in}$ with components $\vec{E}_x$ and $\vec{E}_y$, as specified by the Jones vector:

$$\vec{E}_{in} = \begin{bmatrix} E_x \\ E_y \end{bmatrix} \tag{49}$$

Now imagine that $\vec{E}_{in}$ encounters a simple horizontal linear polarizer which serves to block the $\vec{E}_y$ componet of the wave, while simultaneously allowing $\vec{E}_x$ to pass through unimpeded. We may then express the emergent wave $\vec{E}_{out}$ as another Jones vector:

$$\vec{E}_{out} = \begin{bmatrix} E_x \\ 0 \end{bmatrix} \tag{50}$$

This suggests that we might be able to relate $\vec{E}_{in}$ and $\vec{E}_{out}$ with an appropriate linear transformation, given by some 2×2 matrix $\boldsymbol{J}$,

where $\boldsymbol{J}$ is the *Jones Matrix* characteristic of the horizontal linear polarizer. That is

$$\boldsymbol{J} = \begin{bmatrix} m_{11} & m_{12} \\ m_{21} & m_{22} \end{bmatrix} \tag{51}$$

and

$$\vec{E}_{in} = \boldsymbol{J}\vec{E}_{out} \tag{52}$$

or

$$\begin{bmatrix} E_x \\ E_y \end{bmatrix} = \begin{bmatrix} m_{11} & m_{12} \\ m_{21} & m_{22} \end{bmatrix} = \begin{bmatrix} E_x \\ 0 \end{bmatrix} \tag{53}$$

The components m_{ii} are then easily found, and we find that:

$$\boldsymbol{J} = \begin{bmatrix} 1 & 0 \\ 0 & 0 \end{bmatrix} \tag{54}$$

This approach of using the product of both Jones vectors and Jones matrices to calculate the polarization of emergent electromagnetic waves from linear optical elements is known as the *Jones calculus*, as originally developed by physicist Robert Clark Jones in 1941. It is important to note, however, that the techniques of Jones calculus are only applicable to waves that are already fully polarized, otherwise one must employ the more general (but appreciably more complex) *Mueller calculus*.

v. FINESSE

FINESSE is an optical system simulation developed to design and debug laser interferometers, with the goal of being able to simulate a large variety of user-defined optical configurations. It has a long history stemming from extensive use by a number of optics groups involved in gravitational wave detection.

As gravitational wave and other laser interferometers have become increasingly more powerful and complex, the importance of being able to simulate both the entire interferometer as well as its constituent parts has increased as well.

Assuming a steady state, FINESSE is able to compute the light field amplitudes at every point within a given optical configuration. FINESSE does this by translating the user-defined interferometer into a set of linear equations that it can then solve numerically. The software package *SuiteSparse*, used in FINESSE for solving the large, sparse matrices characteristic of a given system, is perhaps one good example.

A number of standard analyses can be performed automatically by the program. For instance, FINESSE is able to compute modulation-demodulation error signals and transfer functions. Roughly speaking, a transfer function maps a corresponding output value to every possible input value, in an effort to obtain information describing the behavior of various optical components within a given configuration.

FINESSE is also able to perform the analysis using Hermite-Gauss modes, in addition to the regular plane waves we were discussing earlier. Hermite-Gauss modes are approximate solutions to the wave equation, and describe electric field distributions as a product of a Gaussian function and Hermite polynomial. Analyses made using Hermite-Gauss modes allow computation of various optical properties, as well as the effects of mode matching and misalignments.

The program further allows its users to tune every parameter of the interferometer description throughout a simulation, including arm length, mirror reflectivity, modulation frequency, and mirror alignment. Available outputs include a a plot of a photodetector signal as a function of one or two parameters. FINESSE is then able to create either two or three-dimensional plots of output data using the graphics program *Gnuplot*. Additional text ouput may provide additional details regarding the optical configuration, including mode mismatch coefficients, cavity eigenmodes, and beam sizes.

As the complexity of optical systems used in the gravitational wave community have increased significantly over the last several

decades, so too has the necessity to be able to model these systems and other optical configurations. To address this ever-present challenge, the developers of FINESSE have begun working on FINESSE 3.

Owing in no small part to its potential usage in the upcoming Einstein Telescope, the ability to implement the polarization of light in models is but one of several new features scheduled to be included in the upcoming release of FINESSE. The objective then, was to find a way to include polarization within the existing structure of the program.

Utilizing Python, we began by assigning new p and s-polarization variables to the already existent "laser" method. Users would now be able to specify initial field amplitudes for both polarizations upon the implementation of a new laser class in a given optical configuration. FINESSE would then need to be able to calculate two field amplitudes at every point in the system, as opposed to the single amplitude found in previous releases.

What follows are a sampling of some of the different polarization states tested, as represented by the appropriate Jones vector.

Horizontal linearly polarized wave :

$$\boldsymbol{J} = \begin{bmatrix} 1 \\ 0 \end{bmatrix} \tag{55}$$

Vertical linearly polarized wave :

$$\boldsymbol{J} = \begin{bmatrix} 0 \\ 1 \end{bmatrix} \tag{56}$$

Horizontal linearly polarized wave rotated by + 45° :

$$\boldsymbol{J} = \frac{\sqrt{2}}{2} \begin{bmatrix} 1 \\ 1 \end{bmatrix} \tag{57}$$

Horizontal linearly polarized wave rotated by - 45° :

$$\boldsymbol{J} = \frac{\sqrt{2}}{2} \begin{bmatrix} 1 \\ -1 \end{bmatrix} \tag{58}$$

Right-circularly polarized wave:

$$\boldsymbol{J} = \frac{\sqrt{2}}{2} \begin{bmatrix} 1 \\ -i \end{bmatrix} \tag{59}$$

Left-circularly polarized wave:

$$\boldsymbol{J} = \frac{\sqrt{2}}{2} \begin{bmatrix} 1 \\ i \end{bmatrix} \tag{60}$$

In order to determine if FINESSE was indeed successful in modeling our new polarized laser, several optical systems of varying size and complexity were constructed within the program, and the computed light fields compared to what was predicted analytically. This included, among other designs, a simple cavity consisting of a series arrangement of a polarized laser, a partially reflective mirror, and ideal mirror having zero transmission.

We concluded after several trials that FINESSE was indeed capable of computing two linearly independent states of polarization, and as such our next task was to implement a series of polarizers, optical filters which allow the light fields of the two polarizations to be modified. The objective was to create a series of polarized components typical of various optical systems, including both absorptive polarizers, where undesired polarization states are absorbed by the device, and *beam-splitting polarizers*, with unique reflection and transmission coefficients for each polarization.

The components were constructed using classes unique to each individual component, beginning with a simple linear polarizer able to linearly polarize light at any angle specified by the user in degrees.

To accomplish this, we defined a linear polarizer class containing a variable for both a user-defined name and angle.

We then defined a 2×2 array featuring entries consistent with the components of the Jones matrix representative of the polarizer:

$$\boldsymbol{J} = \begin{bmatrix} \cos^2\theta & \sin\theta\cos\theta \\ \sin\theta\cos\theta & \sin^2\theta \end{bmatrix} \tag{61}$$

Owing to the dependence of each of the two outgoing polarizations on each of the two input polarizations, the components of both input fields were coupled to each of the outgoing fields.

Finally, each method featured a nested for-loop that would multiply the appropriate component of the impinging light field by the appropriate component in the array.

With the construction of the new *linear polarizer* class complete, as before the next step involved the construction of a series of optical configurations with which to test it.

This began with a simple p-polarized laser and linear polarizer set to 45 degrees:

Similar to before, we then compared the output fields computed by FINESSE with what what we expected analytically. After some small adjustments to the linear polarizer class, predominantly from small syntax errors, we were able to produce satisfactory light field computations consistent with our previously calculated expectations.

We then implemented a series of other optical configurations featuring our linear polarizer, each time once again comparing field amplitudes computed by FINESSE to what we expected from our own set of calculations.

When we were satisfied that the linear polarizer had been implemented correctly into FINESSE, much of the same process was repeated in implementing circular polarizers, which of course serve to convert linear to circularly-polarized light:

Circular polarizer, right-handed:

$$\boldsymbol{J} = \frac{1}{2}\begin{bmatrix} 1 & i \\ -i & 1 \end{bmatrix} \tag{62}$$

Circular polarizer, left-handed:

$$\boldsymbol{J} = \frac{1}{2}\begin{bmatrix} 1 & -i \\ i & 1 \end{bmatrix} \tag{63}$$

The circular polarizers were then tested and debugged in the same manner as their linear counterparts, using a series of optical arrangements of varying complexities and examining the computed field amplitudes at different points within each system. As before, small adjustments were made as necessary.

The next series of components implemented were a number of *phase retarders*, optical elements which work through the addition of a phase shift between the respective p and s-polarizations of a given light field.

In the physical world, phase retarders typically accomplish this by featuring birefringent uniaxial crystals with one crystal axis of a completely different index of refraction. This unique axis is usually referred to as the *extraordinary axis*, which is then referred to as the *fast* or *slow axis* for the crystal depending on the type of crystal used. Waves propagate with a higher phase velocity along axes with a smaller refractive index (fast axis), whereas the speed of propagation is slower for axes with a higher refractive index (slow axis). Note that any phase retarder with a fast axis equal to either the horizontal or vertical axis can be expressed in the form

$$\boldsymbol{J} = \begin{bmatrix} e^{i\phi_x} & 0 \\ 0 & e^{i\phi_y} \end{bmatrix} \tag{64}$$

where $e^{i\phi_x}$ and $e^{i\phi_y}$ are the resulting phase shifts in $\vec{E}_x$ and $\vec{E}_x$ respectively.

What follows are the Jones matrices for several of the phase retarders implemented into FINESSE:

Quarter-wave plate with vertical fast axis:

$$\boldsymbol{J} = e^{i\pi/4}\begin{bmatrix} 1 & 0 \\ 0 & -i \end{bmatrix} \tag{65}$$

Quarter-wave plate with horizontal fast axis:

$$\boldsymbol{J} = e^{-i\pi/4}\begin{bmatrix} 1 & 0 \\ 0 & i \end{bmatrix} \tag{66}$$

Quarter-wave plate with fast axis rotated by angle θ w.r.t. the horizontal axis:

$$\boldsymbol{J} = e^{-i\pi/4}\begin{bmatrix} \cos^2\theta + i\sin^2\theta & (1-i)\sin\theta\cos\theta \\ (1-i)\sin\theta\cos\theta & \sin^2\theta + i\cos^2\theta \end{bmatrix} \tag{67}$$

Half-wave plate with fast axis rotated by angle θ w.r.t. the horizontal axis:

$$\boldsymbol{J} = e^{-i\pi/2} \begin{bmatrix} \cos 2\theta & \sin 2\theta \\ \sin 2\theta & -\cos 2\theta \end{bmatrix} \tag{68}$$

Much in the same way as before, the phase retarders were then tested using several different optical configurations.

The next component added was the Faraday rotator, an optical component that rotates the plane of polarization using a magnetic field, according to the Faraday effect which describes the behavior of electromagnetic waves in the presence of a magnetic field.

The Jones matrix of the Faraday rotator then takes the form of a simple rotation matrix:

$$\boldsymbol{J} = \begin{bmatrix} \cos\theta & \sin\theta \\ -\sin\theta & -\cos\theta \end{bmatrix} \tag{69}$$

The final component implemented into FINESSE was the polarized beam-splitter,unique among the various components in that it consisted entirely of couplings, in the absence of an array.

The polarized beam-splitter class was designed in much of the same manner as its unpolarized counterpart, consisting of a series of couplings in which both p and s-polarized field amplitudes were computed independently, with their own individual reflection and transmission coefficients.

As we added first the polarized laser, the linear and circular polarizers, the phase retarders, the Faraday rotator, and finally, the polarized beam-splitter, we had access to an increasing number of polarized components with which we were able to build and test real-world optical systems featuring polarization. Two in particular, the Faraday isolator and the previously-discussed Sagnac interferometer, we will now take a closer look at.

The *Faraday isolator* we modelled within the program consisted of a series arrangement of many of the same polarizers we have discussed previously. Isolators are typically featured in optical systems to allow the propagation of light in only one direction along the optical path, and as such it is sometimes referred to as an *optical diode*.

Within our model, a polarized laser is first introduced from the left into the west port of a polarized beam splitter. The beam splitter features p and s reflection and transmission coefficients such that only the p-polarized component of the laser is transmitted through the device and out the east port, whereas the s-polarized component is reflected out the north port, and effectively removed from the isolator entirely.

The now completely p-polarized laser then encounters a Faraday rotator where the plane of polarization is rotated by a 45 degree angle.

Exiting the rotator, the beam then encounters a half-wave plate which acts to change the state of polarization from linear to circular.

Our isolator then features a second polarized beam-splitter identical to the first, with the same geometric orientation and p and s coefficients of reflection and transmission. The beam again enters the west port where only the p-polarization is transmitted out through the east port. The s-polarization is once again reflected out through the north port, and away from the optical axis of the isolator.

Finally an ideal mirror was connected to the east port of out second beam splitter, where the p-polarized component of the laser would be reflected back into the isolator.

We then once again computed light field amplitudes using FINESSE for a number of points within our isolator, and compared to what was expected analytically. After a number of small adjustments, we concluded that our simulated Faraday isolator was indeed working as expected.

The final polarization test we went about implementing was that of the zero-area Sagnac interferometer, with the eventual goal of testing it using a series of signals reminiscent of actual gravitational waves.

We began by defining the variety of components we would need to successfully construct the Sagnac, including ideal and partially reflecting mirrors, three polarized beam splitters,

Figure 1: *The Sagnac interferometer[8].*

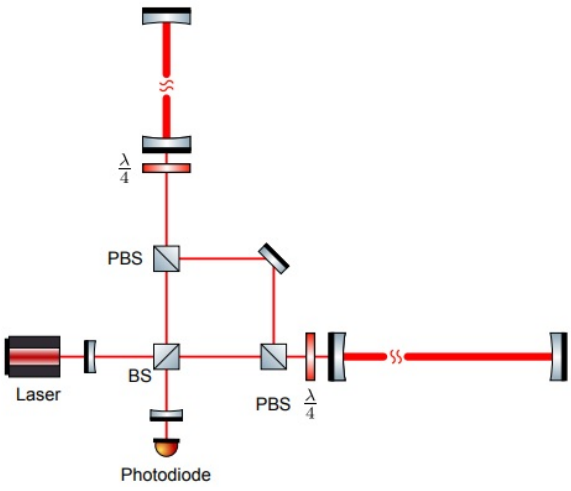

quarter waves plates, and a polarized laser. The components were them arranged as in the figure below.

Note that in order to accommodate the central square loop as seen in the figure, the north port of the PBS1 was connected directly to the east port of PBS2.

Unlike our earlier tests of somewhat simpler polarized optical systems, we unfortunately ran into a number of issues when trying to implement the Sagnac, perhaps most noteworthy the Python-generated error indicating that Suitesparse could not provide an inverse for the appreciably large but sparse matrix for our interferometer.

We tried a variety of approaches in an attempt to isolate the error. By breaking down the Sagnac down into smaller subsystems and then testing them independently, we found that the error most likely resided in the workings of the central square loop.

As of the time of this writing, we are still trying to pinpoint the error but are looking forward to its rectification and future release of FINESSE 3.

The study of gravitional waves has come a long way in the over four decades since Hulse and Taylor's work at Arecibo, and as our efforts to observe them has resulted in the construction of ever more powerful and complex detectors, the need to model and study these very same systems has increased as well. It is to this end that all current and future releases of FINESSE endeavors to achieve.

References

[1] J.M. Weinberg, et al., Timing Measurements of the Relativistic Binary Pulsar PSR B1913+16, (2010) 2.

[2] A. Einstein, Über Gravitationswellen, Sitzungsberichte der Königlich Preussischen Akademie der Wissenschaften Berlin, (1916) 154-167.

[3] B.P. Abbott, et al., (LIGO Scientific Collaboration and Virgo Collaboration), Observation of Gravitational Waves from a Binary Black Hole Merger, (Physical Review Letters) (2016) 2.

[4] B.P. Abbott, et al., GW151226: Observation of Gravitational Waves from a 22-Solar-Mass Binary Black Hole Coalescence (Physical Review Letters) (2016) 2.

[5] C. Bond, et al., Interferometer techniques for gravitational-wave detection (Living Rev Relativ) (2016) 4.

[6] Hartle, J. B., Gravity: An Introduction to Einstein's General Relativity (2003) 331-483

[7] Hartle, J. B., Optics, 4th Ed. (2002) 325-330

[8] M. Wang, et al., Realistic polarizing Sagnac topology with DC readout for the Einstein Telescope (2014) 1-3